Hindawi
Mobile Information Systems
Volume 2023, Article ID 9846319, 1 page
https://doi.org/10.1155/2023/9846319

Retraction

Retracted: Dynamic Fire Monitoring Analysis and Risk Assessment Based on Multisource Satellite Remote Sensing

Mobile Information Systems

Received 13 September 2023; Accepted 13 September 2023; Published 14 September 2023

This article has been retracted by Hindawi following an investigation undertaken by the publisher [1]. This investigation has uncovered evidence of one or more of the following indicators of systematic manipulation of the publication process:

(1) Discrepancies in scope
(2) Discrepancies in the description of the research reported
(3) Discrepancies between the availability of data and the research described
(4) Inappropriate citations
(5) Incoherent, meaningless and/or irrelevant content included in the article
(6) Peer-review manipulation

The presence of these indicators undermines our confidence in the integrity of the article's content and we cannot, therefore, vouch for its reliability. Please note that this notice is intended solely to alert readers that the content of this article is unreliable. We have not investigated whether authors were aware of or involved in the systematic manipulation of the publication process.

Wiley and Hindawi regrets that the usual quality checks did not identify these issues before publication and have since put additional measures in place to safeguard research integrity.

We wish to credit our own Research Integrity and Research Publishing teams and anonymous and named external researchers and research integrity experts for contributing to this investigation.

The corresponding author, as the representative of all authors, has been given the opportunity to register their agreement or disagreement to this retraction. We have kept a record of any response received.

References

[1] J. Chen, W. Zheng, and T. Shan, "Dynamic Fire Monitoring Analysis and Risk Assessment Based on Multisource Satellite Remote Sensing," *Mobile Information Systems*, vol. 2022, Article ID 5039644, 10 pages, 2022.

Hindawi
Mobile Information Systems
Volume 2022, Article ID 5039644, 10 pages
https://doi.org/10.1155/2022/5039644

Research Article

Dynamic Fire Monitoring Analysis and Risk Assessment Based on Multisource Satellite Remote Sensing

Jie Chen, Wei Zheng, and Tianchan Shan

National Satellite Meteorological Center, China Meteorological Administration, Beijing 100081, China

Correspondence should be addressed to Jie Chen; 2016150266@jou.edu.cn

Received 8 June 2022; Revised 25 July 2022; Accepted 16 August 2022; Published 7 September 2022

Academic Editor: Yanyi Rao

In recent years, forest fires have not only destroyed a large amount of vegetation but also the number and burning area of forest fires in the world have increased significantly. In order to reflect the dynamic monitoring analysis and risk assessment of fires in my country in the past 14 years, this paper selects the national terrestrial forest as an area and uses satellite sensing products with a long time series to analyze the time and space of forest burning biomass and forest fires from a qualitative and quantitative perspective. *Feature*. A power-law distribution-based estimation model for forest burning biomass was established, and the accuracy of the estimation results and the interannual variation pattern reached more than 98%, forming the regional sensitivity of the remote sensing evaluation method. With the emergence of new sensors such as NPP-VIIRS and HIGH, the emergence of high-resolution data has enhanced the ability of forest fire area extraction and fire point information identification, which provides more data sources for forest burning NG biomass estimation and forest fire spatial and temporal pattern analysis using these thermal infrared sensors.

1. Introduction

In recent decades, with the impact of global temperature rise and land use change, the number and burning area of global forest fires have increased significantly. Estimating forest burning biomass is the basic condition for studying the carbon emissions released by forest fires, one of the important factors of circulation [1]. As one of the most important resources on Earth, forest is the best habitat for animals and plants; it not only provides a variety of food and rich raw materials for human life but also has the functions of purifying the air, optimizing the environment, reducing noise, and regulating the atmosphere. It can conserve water and soil and reduce the occurrence of natural disasters [2]. Forest fires threaten human life and property safety; at the same time, forest fires change the composition and biodiversity of postfire ecosystems and have important impacts on the carbon balance in the atmosphere and global climate change; the biomass of forest burning and carbon emissions is closely related [3].

In recent years, more and more experts and scholars have used satellite data to estimate forest burning biomass and to analyze impact of carbon emissions from forest fires on global carbon cycle and spatial and temporal characteristics of forest fires [4, 5]. With the emergence of new sensors, such as NPP-VIIRS and high-resolution data, capability of forest fire area extraction and fire point information identification has been enhanced, providing more data sources for forest burning biomass estimation and forest fire spatial and temporal pattern analysis using these thermal infrared sensors. Based on data products from different satellites, the corresponding research method is proposed, which is also a feasible method to use satellite remote sensing technology to monitor spatial and temporal pattern distribution of forest fires and regional sensitivity analysis for a long time and a large area, as well as to estimate biomass consumed by forest fires. At present, domestic and international research tends to use characteristics of thermal infrared remote sensing technology to construct a forest burning biomass estimation model to estimate forest

burning biomass in different regions and forest types for long time series [6].

In this paper, using national MODIS data set of fire trails (MCD45A1) and fire point products (MOD14A2) from 2001 to 2014, we can not only analyze spatial and temporal distribution and occurrence pattern of forest fires in China in past 14 years, which can provide scientific basis for forest fire prevention and decision making in China, but also analyze distribution characteristics of FRP (fire radiative power) in MOD14A2 data, which can provide scientific basis for forest fire prevention and forest change monitoring. The model of remote sensing estimation of forest biomass by forest type can provide scientific decision for forest fire prevention and forest change monitoring; it can also provide a theoretical basis for sustainable development of carbon cycle in China's forest ecosystem, impact of forest fires on atmosphere, global carbon cycle and carbon balance, and estimation of forest carbon sinks [7]. It is also important for the study of global carbon cycle and carbon balance and estimation of forest carbon sink, etc.

2. Related Work

With the emergence and application of satellite remote sensing technology, experts and scholars at home and abroad have also carried out methods to study distribution of forest fires and regional sensitivity evaluation using satellite remote sensing data [8]. The fire points extracted from MODIS data were compared with historical fire traces; it was found that fire points of two categories, 8 and 9, extracted from MOD14A1 (daily level 31 km fire hotspot produce), were suitable for forest fire monitoring, and agreement with field survey data was as high as 0.83; and fire points of two categories, 8 and 9, extracted from MOD14A1, were used. The results show that most likely fire season is April and May in spring, followed by autumn, and mainly in September. In terms of spatial location, most fire-prone area is Daxinganling, which accounts for 64.74% of province's forest burned area; Xiaoxinganling is second, accounting for 23.49% [9]. Using MCD45A1 data, a logistic forest fire risk model was established, and forest fire risk level in province was studied in terms of time and space, and finally level of forest fire occurrence was classified into five areas, including no fire risk area, low fire risk area, medium fire risk area, high fire risk area, and very high fire risk area [10]. This paper introduces the development of four forest fire monitoring satellites, including FY-ID satellite, NOAA series weather satellite, and EOS series satellites (TERRA, AQUA), and analyzes the forest fire points [11]. Spatial analysis was conducted using MODIS14A2 with three environmental factors: elevation, average annual precipitation, and average annual temperature at different levels. The results showed that annual forest fire area in China showed a decreasing trend, but interannual variation of area of fire trails was large, and area of fire trails in provinces of South China and Southwest China was more serious in recent years; monthly fluctuations of forest fires were also more. The monthly fluctuations of forest fires are also obvious, with the largest area of burned land in March, and southern, southwestern, northwestern, and northeastern regions are sensitive to monthly changes [12]. Using TM data of long time series in last 20 years, NDVI data with fire trails were used to fit equation to obtain NDVI fire trails reading values, and long-time fire trails were discriminated by NDVI images and queue values to analyze fire trails [13]. The spatial analysis of burned areas was carried out using MCD45A1 data, and distribution of forest burned areas was confirmed to be mainly in range of 50°~55°[14]. SPOT-VGT and MOD14 data were used to calculate fire trails in northern Eurasia in terms of time series [15]. Forest fires were updated and counted and analyzed using ETM and MODIS data, i.e., canopy cover and forest cover loss were estimated using ETM to determine forest fire disturbance; meanwhile, MODIS data were used to estimate the area of interpreted fire trails.

In this paper, we use fire product data (MOD14A2) and fire trails product data (MCD45A1) from MODIS during 2001–2014, as well as background data such as vegetation distribution maps and administrative divisions to explore quantitative estimation of forest burning biomass by satellite remote sensing on a national land scale with four forest types in China as the study area [16]. We also analyzed location, area, and vegetation types of forest fires in China and formed a quantitative remote sensing estimation method for annual forest consumption biomass of different forest types; analyzed MODIS fire monitoring data covering China on a daily basis to reveal forest fires in China in past 14 years (2001–2014); and formed a quantitative remote sensing estimation method for forest fires in China.

3. Forest Burning Biomass Estimation Model

Figure 1 shows the technical route of national annual forest burning biomass estimation, which mainly consists of analyzing characteristics of FRP curtain law, constructing FRE estimation model according to different forest types and solving values of parameters in model and correction values; finally, forest burning biomass is estimated according to experimental conversion coefficients, and the area of burned traces of MCD45A1 time series data set of four forest types extracted from eight vegetation climate zones is used. The data were compared and validated with model method of forest fire emission calculation. Figure 2 shows the technical roadmap of the national distribution pattern study, which mainly takes different years, months, and regions as research objects and conducts spatial analysis to summarize forest fire pattern distribution pattern by area, burning type, spatial distribution, and temporal distribution in the past 14 years in China. Figure 3 shows the remote sensing analysis method to obtain regional sensitivity evaluation of forest fires through comparison of single and comprehensive indicators.

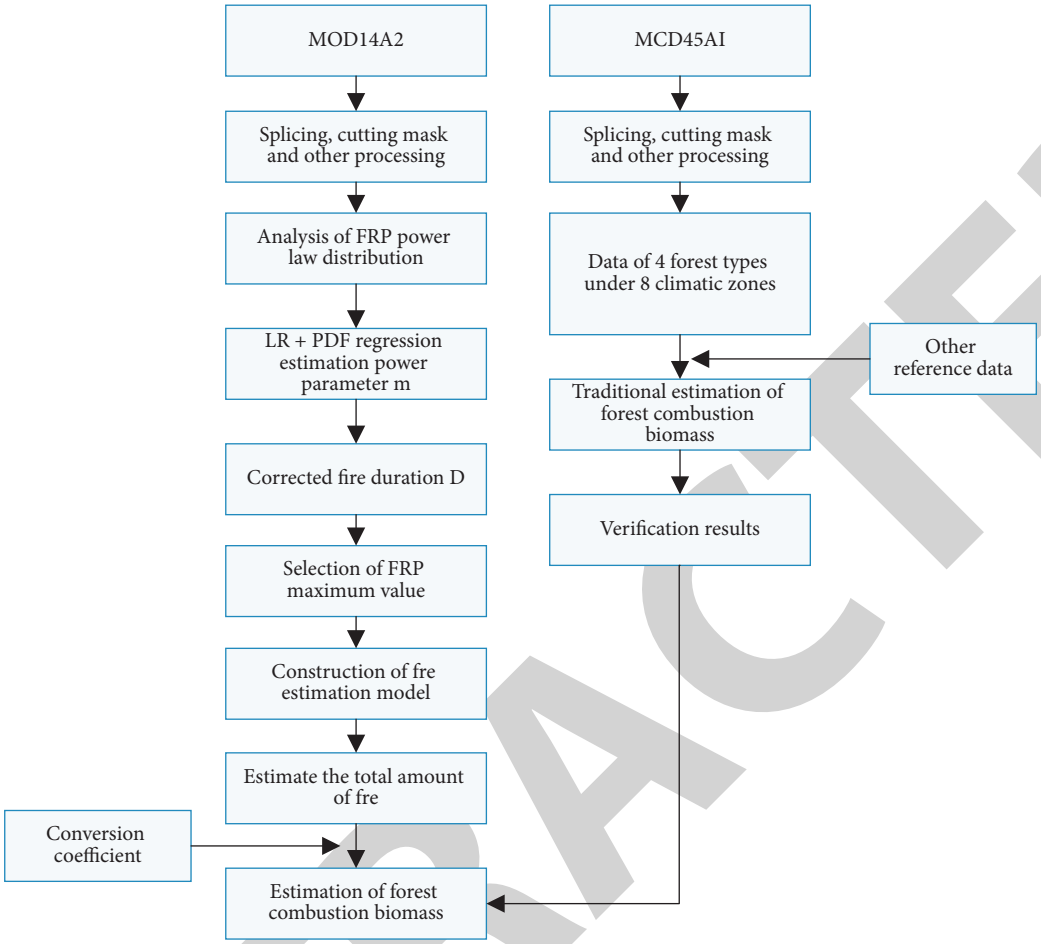

Figure 1: Flow chart of forest burning biomass estimation technology.

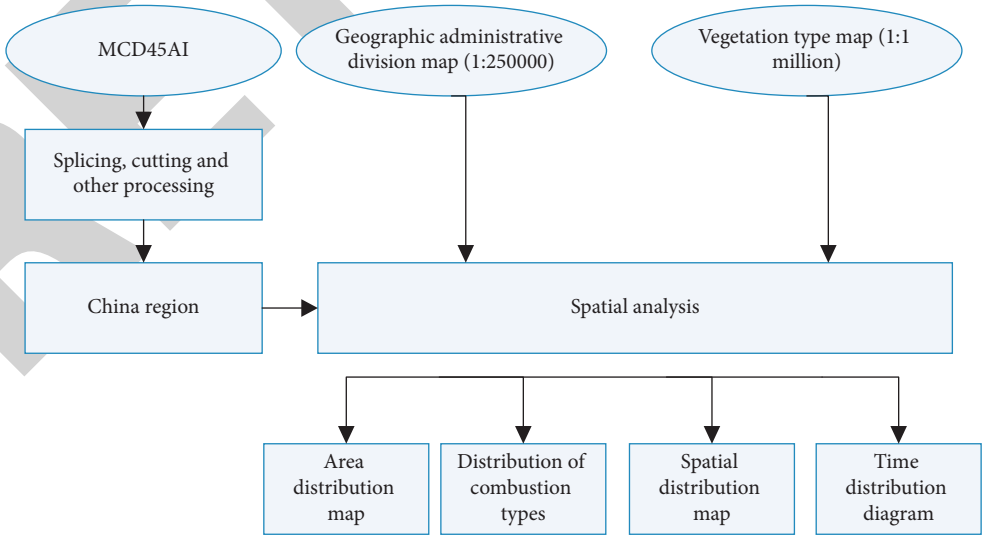

Figure 2: Schematic diagram of the overall technical process of spatial and temporal pattern distribution pattern of forest fires nationwide.

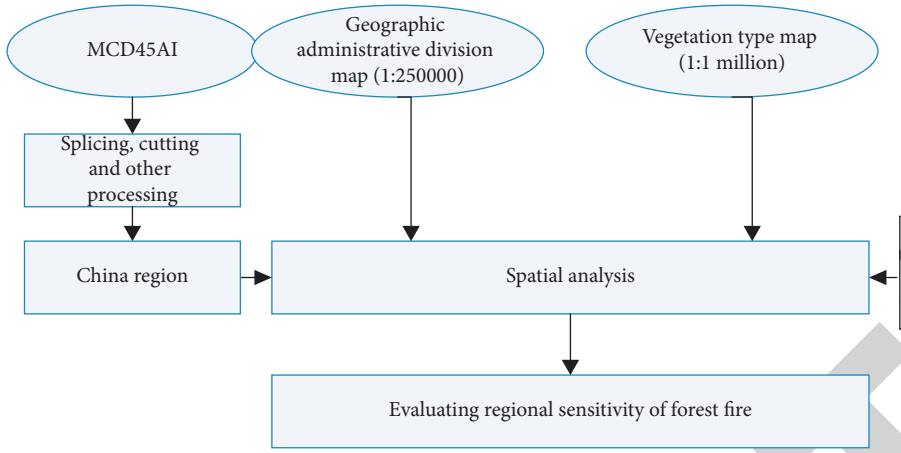

Figure 3: Schematic diagram of the overall technical process of regional sensitivity analysis of forest fires nationwide.

4. Power-Law Distribution Algorithm

When FRP (unit: W) can be measured continuously in ideal state, total fire radiation energy, FRE (unit: J), is defined in the following form (Kumar et al, 2011):

$$FRE = \int_{t=0}^{t-d} FRP(t)dt, \tag{1}$$

where d is fire duration (unit: s).

For discrete FRP values, assuming that there is sufficient time to draw samples of FPR and there is a linear variation between successive samples of FRP, the corresponding FRE can be estimated by the gradient numerical integration method, which is defined in the following form:

$$FRE_{mum.int} \approx \sum_{i=1}^{i-n} \frac{(t_{i+1} - t_i)(FRP_{i+1} + FRP_i)}{2}, \tag{2}$$

n is the total number of FRPs measured during fire duration. Assuming equal time intervals, (2) can be deformed as follows:

$$FRE \approx d \sum_{i=1}^{i=n} \frac{FRP_i}{n}, \tag{3}$$

where d is fire duration. Since d in the expression is replaced by $n\Delta t$ for equal time intervals, and FRP time interval is assumed to be measured continuously, (3) can be defined as expectation value for solving FRE as follows:

$$FRE = dFRP, \tag{4}$$

where FRP is the expectation for duration of fire d.

According to the statistical principle, when the sample size of FRP is small, the arithmetic mean and expected value will be very different. The above derivation process is the traditional FRE estimation method, which is carried out under ideal conditions, while in the reality fire radiance rate (FRP) fluctuates greatly, and results of gradient numerical integration for FRE are very sensitive to FRP of satellite sampling, which is missing and insufficient. Satellite data provide the only way to monitor ground fires in large areas, but due to long transit time interval of polar orbiting satellites, there are missing and insufficient samples of fires being monitored in time variation; so, many experts and scholars are studying method of solving FRE by extrapolating FRP data. In this paper, FRE is estimated by using curtain function based on distributional characteristics of curtain law function of FRP in temporal variation, and the probability density function of curtain function has the following form:

$$P_{(x)} = cx^{-m}, \tag{5}$$

where $P_{(x)}$ is the probability density function of power-law distribution, X is a continuous variable, C is a constant, and m is the power parameter.

The arithmetic mean of sample data for a power-law distribution cannot be used as an estimate of its expectation, especially in case of small sample sizes (Newman, 2005). Therefore, the expected value of power function is derived by the following analysis. First, we integrate all probability density functions, and the sum of integrals is 1, so that a relationship between constant c and power parameter m is obtained.

$$\int_{x_{miv}}^{x_{max}} p(x)d(x) = \int_{x_{miv}}^{x_{mix}} cx^{-m}d(x) = 1, \tag{6}$$

$$c = (I - m)\left(\frac{I}{x_{max^{-m+1}} - x_{min^{-m+1}}}\right). \tag{7}$$

Then, the expected value of x is calculated:

$$\begin{aligned} \exp(x) &= x \\ &= \int_{x_{min}}^{x_{sex}} p_{(x)} x d(x) \\ &= \int_{x_{mix}}^{x_{mux}} cx^{-m+1} d(x) \\ &= (1-m)\left(\frac{1}{x_{max^{-m+1}} - x_{min^{-m+1}}}\right)\left(\frac{x_{max^{-m+2}} - x_{min^{-m+2}}}{2-m}\right). \end{aligned} \tag{8}$$

Assuming that FRP follows a power-law distribution during the fire duration$x$ in (8) is replaced by FRP, and the form (4) is combined to obtain (9):

$$E_{pourrlaw} = dFRPFR$$

$$d(I-m)\left(\frac{I}{FRP_{\max^{-m+1}} - FRP_{\min}^{-m+1}}\right)\left(\frac{FRP_{\sin^{-\sin+2}} - FRP_{\min^{-m+2}}}{2-m}\right), \tag{9}$$

where d is fire duration, $FRP_{\max}$ is maximum value of FRP, and $FRP_{\min}$is minimum value of FRP.

In estimating the FRE value, the power function cumulative probability distribution calculation method of (9) has another choice compared with the traditional gradient numerical integration method of (2). From (9), we can easily find that $FRE_{pourrlaw} = 0$ when $m = 1$, $FRE_{pourrlaw}$ is meaningless when $m = 2$, $FRP_{\max}$ and $FRP_{\min}$are meaningful only when $m < 2$ or $m > 2$, and $FRP_{\max}$ and $FRP_{\min}$ play a decisive role in $FRE_{pourrlaw}$.

(1) Forest burn rate: in order to better evaluate the extent of forest hazards and objectively compare sensitivity of forest fires between regions, forest burn rate is introduced and calculated as follows:

$$R_f = \frac{D_{to}}{D_{fa}}, \tag{10}$$

where $D_{ba}$is the average annual forest fire area of a city and D_{fa} is the annual forest area of a city.

(2) Forest overfire area ratio

It reflects regional characteristics of forest fires. Comparing the national average with forest fire hazard of each province (city), the formula is as follows:

$$R_{ba} = \frac{D_{ba}}{C_{ba}}. \tag{11}$$

In order to better reflect forest fire control ability of a region, the coefficient of variation of forest fire area is introduced. If the forest fire control ability of a region is better, then the coefficient of variation of forest fire area in that region is smaller, which means that the forest fire management level of that region is better. In particular, when comparing two adjacent periods, if the coefficient of variation of the former period is larger than that of the latter period, it proves that the control ability of forest fires in the latter period has been improved and the management level has been enhanced, which is calculated as follows:

$$V_n = \frac{\sigma_{ba}}{M_{ba}} \times 100\%, \tag{12}$$

where σ_{ba} is the standard deviation of annual average forest fire area in a province (city) and M_{ba} is the average annual average forest fire area in province (city).

5. Results

When estimating forest biomass consumed by a single forest fire using curtain law distribution characteristics of FRP, no correction for fire duration d is necessary; however, when estimating forest burning biomass on an annual basis, duration d must be corrected to eliminate the error caused by it. The parameters and results for calculating fire durations of three forest types are shown in Tables 1–3, using nine typical fires in broadleaf forest in 2003, coniferous forest in 2009, and shrub forest in 2005, respectively. The incremental ratio (ABB) to real fire duration d set of data monitored by satellite was obtained, and regressions were fitted to these data, and fitting results are shown in Figures 4–6.

The relationship between fire duration d and incremental forest biomass ratio is shown in Figure 4. Assuming the whole year as the real time of satellite monitoring, the error value of the incremental ratio of broadleaf forest in 2003 was solved in the relationship equation, and then the error value of the incremental ratio was brought into (12) to calculate the time correction coefficient of forest burning biomass for the whole year. This is used as an example to correct the fire duration d of broadleaf forest year by year.

The relationship between fire duration d and incremental forest burning biomass ratio for coniferous forests is shown in Figure 5. Assuming whole year as real time of satellite monitoring, error value of incremental ratio of coniferous forest in 2009 was solved in relationship equation, and then error value of incremental ratio was applied to (12) to calculate time correction coefficient of forest burning biomass for whole year. As an example, fire duration of coniferous forest was corrected year by year d.

The relationship between fire duration d and incremental forest biomass ratio is shown in Figure 6. The error value of incremental ratio of shrubland in 2005 was solved by assuming the whole year as real time of satellite monitoring, and then the error value of incremental ratio was applied to (12) to calculate the time correction coefficient of forest burning biomass for the whole year. This is used as an example to correct the fire duration of shrubland year by year (d).

In this paper, we analyze the effect of the selection of the maximum FRP value on estimation results from FRP data. Here, a typical fire in a broadleaf forest in 2003 was selected as an example, and the influence of maximum FRP value on estimated forest burning biomass was analyzed, while other parameters were kept constant. The analysis was carried out by keeping the minimum value of FRP and other parameters in Table 4 constant and analyzing effect of different maximum values of FRP on estimation results. The maximum value was incremented by 10%, and each increment of forest burning biomass was calculated, resulting in two sets of data: incremental difference of FRP maximum value ($\Delta FRP_{\max}\%$) and incremental difference of forest burning biomass ($\Delta BB\%$) (as in Table 4).

As shown in Figure 7, using two sets of data formed by incremental difference of FRP maximum ($FRP_{\max}\%$) and incremental difference of forest burning biomass ($\Delta BB\%$), the equation relationship equation was established, and model parameters were regressed using SAS statistical software, the P value of slope was less than 0.0001, i.e., independent variable was significant, while intercept $P = 0.0379$, i.e., constant term was not significant

Table 1: Examples of correction durations d for broadleaf forests.

Lat	Lon	Fire duration	Scaling, m	FRP_{max}	FRP_{min}	BB_{really}(T)	d+365 × 24(h)	$BB_{increase}$(T)	$\Delta BB=(BB_{increase}-BB_{really})/BB_{really}$
47.5	87.2	21.9	1.708	326.2	19.8	1965	8842.4	817541	416.2
48.7	121.7	50.1	1.702	179.1	21.9	3856	8475.2	685247	176.2
27.3	92.6	120.2	1.7041	143	13.2	6847	8835.5	465247	72.41
25.4	114.1	85.1	1.7048	137.5	12.3	4125	8471.2	425366	102.3
50.7	120.5	125.7	1.7087	135.2	10.9	8475	8593.5	852474	380.2

Table 2: Examples of correction durations d for coniferous forests.

Lat	Lon	Fire duration	Scaling m	FRP_{max}	FRP_{min}	BB_{really}(T)	d+365 × 24(h)	$BB_{increase}$(T)	$\Delta BB=(BB_{increase}-BB_{really})/BB_{really}$
27.5	112.2	11.9	1.708	126.2	12.8	965	8742.4	417541	716.2
23.7	101.7	50.1	1.708	109.1	19.9	4856	8875.2	585247	176.2
23.3	98.6	78.2	1.708	643	33.2	4847	8935.5	565247	122.41
22.4	104.1	75.1	1.708	537.5	42.3	4525	8571.2	625366	302.3
51.7	110.5	102.7	1.708	635.2	11.9	5475	8893.5	752474	180.2

Table 3: Examples of shrubland correction durations (d).

Lat	Lon	Fire duration	Scaling m	FRP_{max}	FRP_{min}	BB_{really}(T)	d+365 × 24(h)	$BB_{increase}$(T)	$\Delta BB=(BB_{increase}-BB_{really})/BB_{really}$
233.5	162.2	81.9	1.908	36.2	6.8	1065	8142.4	117541	116.2
24.7	151.7	70.1	1.908	119.1	5.9	2856	8275.2	285247	96.2
24.3	108.6	78.2	1.908	443.9	13.2	3847	8435.5	365247	132.41
25.4	134.1	75.1	1.908	437.5	17.3	2525	8571.2	425366	242.3
21.7	160.5	92.7	1.908	635.2	21.9	3475	8293.5	652474	103.2

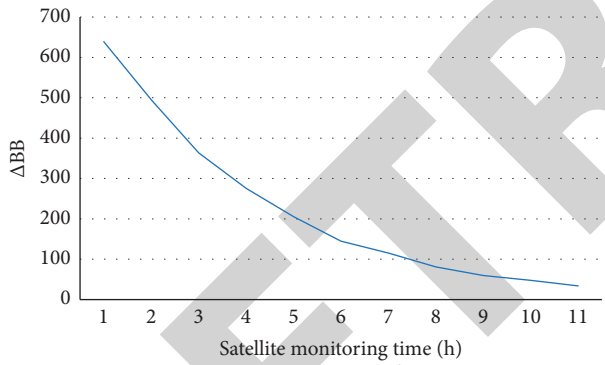

Figure 4: Modified relation for duration d in broadleaf forest.

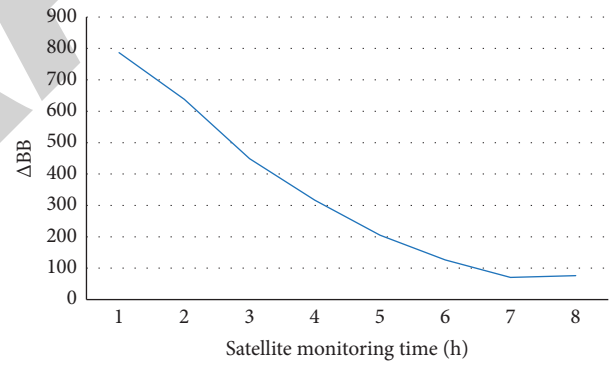

Figure 5: Modified relationship for coniferous forest duration.

($P = 0.0379 > 0.0001$), but by the significance of slope, it can be seen that there is a positive correlation between selection of maximum value of FRP and estimation error.

Similarly, a typical fire in broadleaf forest in 2003 was selected as an example to analyze influence of selection of the minimum FRP value on estimation accuracy. The maximum value of FRP and other parameters were kept constant, and only the effect of different minimum values of FRP on estimation results was analyzed. The minimum value was incremented by 10%, and each increment of forest burning biomass was calculated, resulting in two sets of data: incremental difference in FRP minimum (FRP_{max}%) and incremental difference in forest burning biomass (ΔBB%) (see Table 5).

As shown in Figure 8, using two sets of data formed for incremental difference of FRP minimum (FRP_{max}%) and incremental difference of forest burning biomass (ΔBB %), relationship equation was established, and the same model parameters were regressed using SAS statistical software; P value of slope was less than 0.0001, that is, independent variable was significant; however, intercept $P = 0.0331$, that is, the constant term was not significant ($P = 0.0331 > 0.0001$), but by the significance of slope, it can be seen that there is also a positive relationship between the selection of minimum value of FRP and estimation error.

Figure 9 visualizes differences and interannual variation of two methods for estimation of forest burning biomass in last 14 years. The dashed and solid lines show interannual variation trends of forest fire emission calculation model and curtain-law distribution-based method, respectively. From trends of three forest types, we can see that interannual variation patterns of two methods are obvious and can reflect fluctuation of forest burning biomass from year to year. The estimated burning biomass of three forest types in

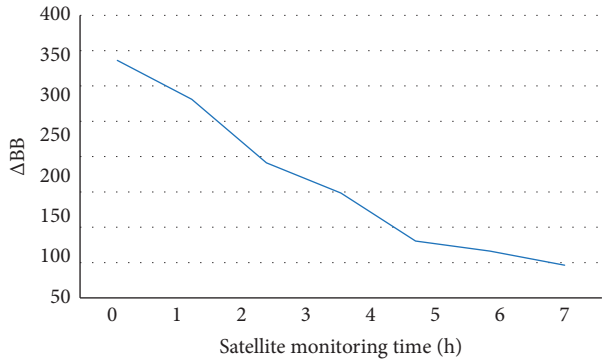

Figure 6: Modified relation for shrubland duration.

Table 4: FRP_{max} example data of effect of selection on estimation accuracy.

Time	M	FRP_{max}	FRP_{min}	BB (Tg)	ΔFRP_{max}, %	ΔBB, %
13.5	1.745	160.9	31	1180	0	0
13.5	1.745	176.9	31	1232	9	5
13.5	1.745	192.9	31	1230	21	9
13.5	1.745	208.9	31	1236	29	13
13.5	1.745	235.7	31	1365	61	24

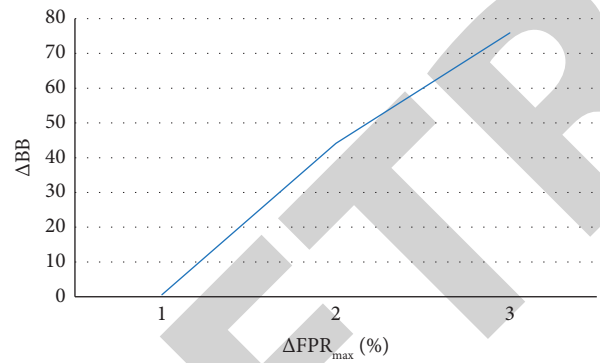

Figure 7: FRP_{max} effect on accuracy of estimated combustion biomass.

Table 5: Example data for effect of FRP_{min} selection on estimation accuracy.

Time	M	FRP_{max}	FRP_{min}	BB (Tg)	ΔFRP_{max}, %	ΔBB, %
13.5	1.745	160.9	31	1780	0	0
13.5	1.745	160.9	30	1523	9	5
13.5	1.745	160.9	32	1830	25	10
13.5	1.745	160.9	36	1836	32	20
13.5	1.745	160.9	34	1965	60	30

2014 based on the curtain-law distribution method is decreasing, which is in line with decrease or basically the same number of forest overfire area and occurrence in 2014 compared with 2013 as announced by National Bureau of Statistics (as shown in Figure 10); however, results calculated by forest fire emission calculation model are increasing,

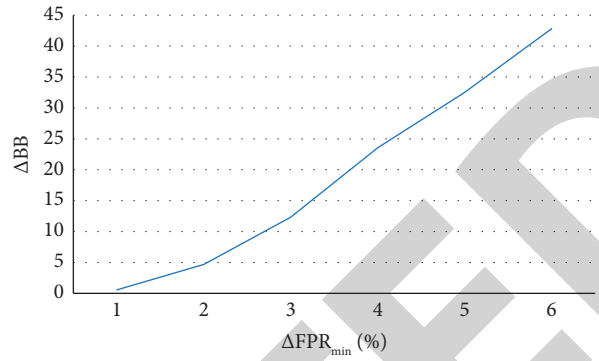

Figure 8: Effect on accuracy of estimated combustion biomass.

which indicates that the interannual variation pattern of estimated results based on the curtain-law distribution method is more consistent with the interannual variation of forest biomass consumed by forest fires in China which is more consistent with interannual variation of forest biomass. Secondly, interannual variation of the curtain-law distribution method fluctuates within the same order of magnitude, while the variation of forest fire biomass in some years is not within the same order of magnitude, and variation of forest fire biomass from millions to tens of millions of tons in adjacent years is not consistent with forest fire biomass consumption in China, according to the comparison of number of forest fires and fire area published by the National Bureau of Statistics.

In this paper, FRP of broad-leaved forest, coniferous forest, and shrub forest has the characteristic of curtain-law distribution, and forest burning biomass model was established by the forest type. The interannual variation of forest fire emission model and estimation of forest burning biomass based on curtain law distribution can be compared and analyzed, and it can be concluded that interannual variation of estimation results based on curtain law distribution fluctuates within the same order of magnitude, and the interannual variation pattern is consistent with characteristics of forest fires in China in past 14 years. However, interannual variation of forest fire emissions was several tens of times larger than the variation of adjacent years and even larger than 14-year total estimated based on curtain-law distribution (Figure 10). In addition, the problem of estimating annual forest burning biomass in large areas using the forest fire emission calculation model is that it is difficult to accurately obtain the annual fire site area, forest combustible load, and burning coefficient. It is difficult to survey the area of forest fire sites in large areas and for a long time, and it is also difficult to measure some high mountains. In addition, using the average of product of forest combustible load and burning coefficient instead of the actual value of two parameters for each year, estimation of forest burning biomass for a long time series often leads to large errors. In this paper, we use thermal infrared remote sensing to detect energy emitted from ground and curtain-law distribution of FRP of fire to build a curtain-law distribution-based estimation model by the forest type so as to estimate forest burning biomass in a large area and a long time series;

Figure 9: Interannual variation of burning biomass for three forest types. Note: subplots A, B, and C show comparison of interannual variation patterns of estimated burning biomass in broad-leaved forests, coniferous forests, and shrublands, respectively.

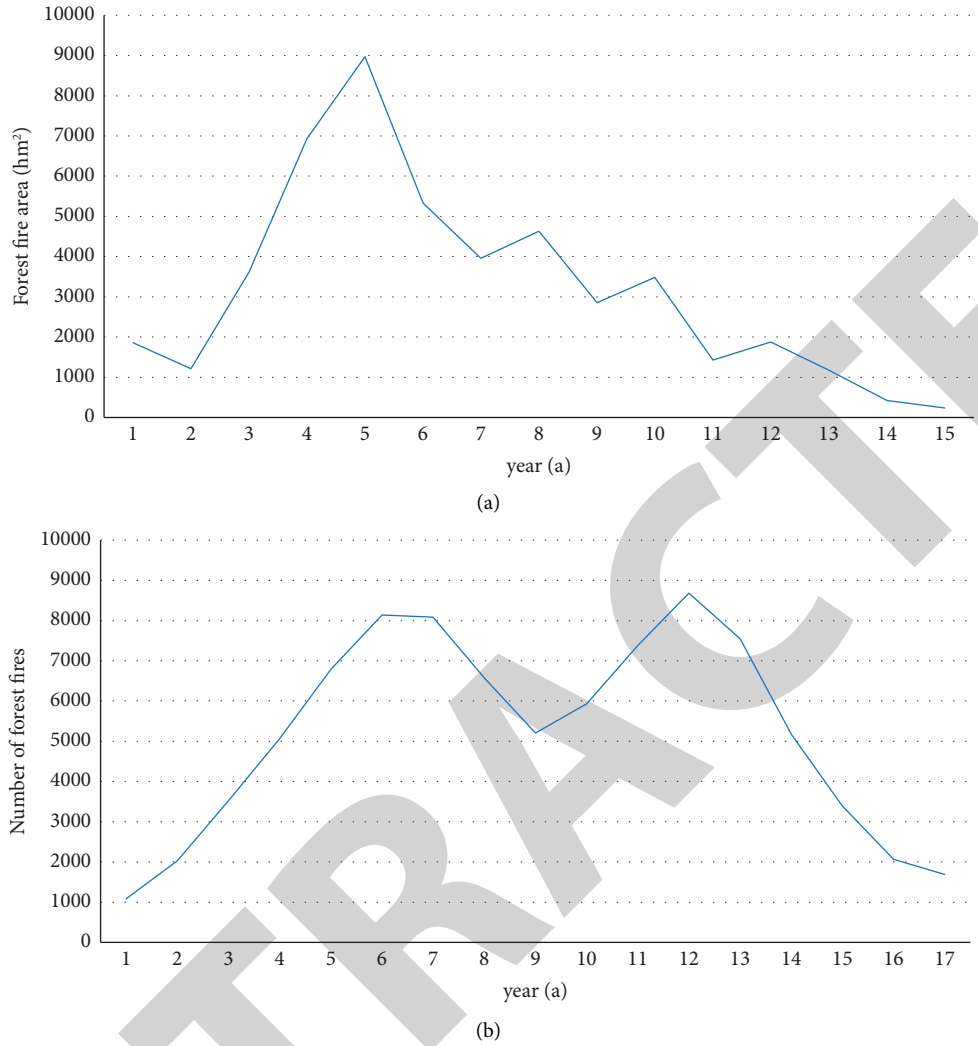

Figure 10: Interannual variation of forest fire data published by National Bureau of Statistics.

compared with parameter acquisition of the forest fire emission calculation model, parameters in the model are directly from satellite data, and no field survey is required. Compared with parameters of the forest fire emission calculation model, parameters in the model are directly derived from satellite data, which can reduce errors caused by human factors and save time and effort.

6. Conclusions

With development of satellite remote sensing technology and its applications, use of long time series of satellite fire monitoring product data to estimate forest burning biomass in large areas and to evaluate distribution patterns of spatial and temporal characteristics of forest fires nationwide provides a new and effective technical means. Therefore, in this paper, spatial and temporal characteristics of forest fires and estimation of forest burning biomass in a large area are investigated by using remote sensing data sources. Using spatio-temporal curtain law distribution characteristics of FRP, we established a model for estimating burning biomass of different forest types in a large area by broad-leaved forest, coniferous forest, and shrub forest, and accuracy of estimation results by using forest fire emission calculation model is more than 98%, which provides a real time and effective method for estimating forest burning biomass and evaluating the spatio-temporal distribution law of forest fires in long time and large area. The results were 98% accurate.

Data Availability

No data were used to support this study.

Conflicts of Interest

The authors declare that there are no conflicts of interest with any financial organizations regarding the material reported in this manuscript.

Acknowledgments

This study was supported by the National Key R&D Program of China (2021YFC3000300).

References

[1] M. Kganyago and L. Shikwambana, "Assessment of the characteristics of recent major wildfires in the USA, Australia and Brazil in 2018–2019 using multi-source satellite products," *Remote Sensing*, vol. 12, no. 11, p. 1803, 2020.

[2] B. Koetz, F. Morsdorf, S. Van der Linden, T. Curt, and B. Allgöwer, "Multi-source land cover classification for forest fire management based on imaging spectrometry and LiDAR data," *Forest Ecology and Management*, vol. 256, no. 3, pp. 263–271, 2008.

[3] M. A. Wulder, S. M. Ortlepp, J. C. White, N. C. Coops, and S. B. Coggins, "Monitoring tree-level insect population dynamics with multi-scale and multi-source remote sensing," *Journal of Spatial Science*, vol. 53, no. 1, pp. 49–61, 2008.

[4] H. Taubenböck, M. Wurm, M. Netzband et al., "Flood risks in urbanized areas–multi-sensoral approaches using remotely sensed data for risk assessment," *Natural Hazards and Earth System Sciences*, vol. 11, no. 2, pp. 431–444, 2011.

[5] K. Xu, X. Zhang, Z. Chen, W. Wu, and T. Li, "Risk assessment for wildfire occurrence in high-voltage power line corridors by using remote-sensing techniques: a case study in Hubei Province, China," *International Journal of Remote Sensing*, vol. 37, no. 20, pp. 4818–4837, 2016.

[6] N. M. de Musso, D. Capolongo, A. Refice, F. P. Lovergine, A. D'Addabbo, and L. Pennetta, "Spatial evolution of the December 2013 Metaponto plain (Basilicata, Italy) flood event using multi-source and high-resolution remotely sensed data," *Journal of Maps*, vol. 14, no. 2, pp. 219–229, 2018.

[7] J. Lai, J. Zhu, Y. Xie, P. Wang, W. Li, and L. Fu, "Understanding China's resumption of work and production during the critical period of COVlD-19 based on multi-source data," *Transactions in GIS*, vol. 26, no. 2, pp. 1062–1079, 2022.

[8] Q. Zheng, Y. Zeng, J. Deng, K. Wang, R. Jiang, and Z. Ye, "Ghost cities identification using multi-source remote sensing datasets: a case study in Yangtze River Delta," *Applied Geography*, vol. 80, pp. 112–121, 2017.

[9] A. O. Amoakoh, P. Aplin, K. T. Awuah et al., "Testing the contribution of multi-source remote sensing features for random forest classification of the greater amanzule tropical peatland," *Sensors*, vol. 21, no. 10, p. 3399, 2021.

[10] F. Bioresita, A. Puissant, A. Stumpf, and J. P. Malet, "Fusion of Sentinel-1 and Sentinel-2 image time series for permanent and temporary surface water mapping," *International Journal of Remote Sensing*, vol. 40, no. 23, pp. 1–24, 2019.

[11] X. Bai, P. Du, S. Guo et al., "Monitoring land cover change and disturbance of the mount wutai world cultural landscape heritage protected area, based on remote Sensing time-Series images from 1987 to 2018," *Remote Sensing*, vol. 11, no. 11, p. 1332, 2019.

[12] D. Ruelland, A. Tribotte, C. Puech, and C. Dieulin, "Comparison of methods for LUCC monitoring over 50 years from aerial photographs and satellite images in a Sahelian catchment," *International Journal of Remote Sensing*, vol. 32, no. 6, pp. 1747–1777, 2011.

[13] M. S. Tehrany, S. Jones, F. Shabani, F. Martínez-Álvarez, and D. Tien Bui, "A novel ensemble modeling approach for the spatial prediction of tropical forest fire susceptibility using LogitBoost machine learning classifier and multi-source geospatial data," *Theoretical and Applied Climatology*, vol. 137, no. 1-2, pp. 637–653, 2019.

[14] D. Liu, L. Wang, Y. Sun, and S. Lian, "MRS-STFF: evaluation of biomass energy combustion and associated pollutants," *Human and Ecological Risk Assessment: An International Journal*, vol. 28, no. 2, pp. 222–242, 2022.

[15] M. Rättich, S. Martinis, and M. Wieland, "Automatic flood duration estimation based on multi-sensor satellite data," *Remote Sensing*, vol. 12, no. 4, p. 643, 2020.

[16] Q. Chen, M. Ding, X. Yang, K. Hu, and J. Qi, "Spatially explicit assessment of heat health risk by using multi-sensor remote sensing images and socioeconomic data in Yangtze River Delta, China," *International Journal of Health Geographics*, vol. 17, no. 1, 15 pages, 2018.